Turkish Journal of Electrical Engineering & Computer Sciences

http://journals.tubitak.gov.tr/elektrik/

Research Article

Turk J Elec Eng & Comp Sci
(2016) 24: 3524 – 3542

doi:10.3906/elk-1404-425

Modeling and performance optimization of photovoltaic and thermal collector hybrid system

Dilşad ENGİN[1,*], **Metin ÇOLAK**[2]

[1]Department of Control and Automation Technology, Ege Higher Vocational School, Ege University, Bornova, İzmir, Turkey

[2]Department of Electrical and Electronics Engineering, Faculty of Engineering, Ege University, Bornova, İzmir, Turkey

Received: 15.04.2014 • **Accepted/Published Online:** 14.05.2015 • **Final Version:** 20.06.2016

Abstract: In this paper, the hybrid photovoltaic/thermal collector (PV/T) system's electrical and thermal efficiency was examined by stating a mathematical model and developing a prototype of the system. To enhance the electrical efficiency, the cell temperature of the PV module was decreased with cooling and the heated fluid could be used for low heating applications. For this purpose, a PV/T system was modeled and constructed using a thermal collector placed beneath the photovoltaic panel where the excess heat and solar radiation through the transparent PV module was the input of the thermal collector. A transparent solar module was used in order to improve the total efficiency of the hybrid PV/T system by means of increasing the radiant solar energy reaching the absorber plate of the collector. The absorber plate was coated with titanium dioxide as the absorption level of the coating was higher than 95%, which increases the thermal output by 10%. We note that using TINOX coating for the absorber plate and transparent solar module had the advantage of increasing the thermal yield of the hybrid system. The influences of the dynamic parameters on the system performance, wind speed and water flow rate, were examined on a daily basis and it was observed that the wind speed had a minor effect on the performance and that forced circulation improved the thermal efficiency. The PV/T hybrid system was compared with the separate PV module and thermal collector efficiencies and the results are presented. With these improvements, the efficiency of the single cover, water type PV/T hybrid system is increased to the maximum reported value in literature.

Key words: Solar cell, solar collector, photovoltaic/thermal hybrid system, optimization, efficiency

1. Introduction

The awareness of the effects of global warming, mostly caused by CO_2 emission, has led to a search for ways of obtaining power from alternative energy sources such as wind, solar, and microhydro. Among the renewable energy sources, solar power is widely used, especially for producing heat energy. These systems are used to provide hot water requirements as well as for indoor heating. Electrical energy is generated from solar energy using solar modules and arrays. Production of heat and electricity by the same unit has been the main idea of many researches. It is a known fact that most of the solar radiation absorbed by the solar cells is not converted into electrical energy, but it increases the cell temperature, whereas increased cell temperature decreases the electrical efficiency. In order to obtain a higher efficiency, this heat should be extracted from the cells during operation. As the photovoltaic conversion efficiency is a decreasing linear function of temperature, the cooled

*Correspondence: dilsad.engin@ege.edu.tr

solar cell power output increases. The heated fluid may also be used for low heating applications. This phenomenon is the main idea of this paper.

A combined solar cell and thermal collector system, called a photovoltaic/thermal (PV/T) hybrid system, that produces electrical energy as well as low temperature hot water, could be an alternative to the use of single solar modules. The incident solar radiation on the solar module is converted to electrical energy, while the absorber plate beneath the module absorbs the excess heat. The absorber plate may or may not be in thermal contact with the solar module. In both scenarios the excess is used as an input. A heat carrier fluid, especially water, removes this excess heat from the absorber plate and the solar cells, thus increasing the electrical efficiency and the electrical output of the PV/T system.

2. Literature review and project approach

Various theoretical and experimental studies have been performed on PV/T hybrid systems since the 1970s. In order to optimize the energy output of the PV/T hybrid systems, there has been much research over the last 20 years. Authors' approaches to PV/T systems vary, but these systems are usually investigated in 2 main categories, as water-hybrid and air-hybrid collectors. Some of these studies have been performed using water [1–13] and dual (water and air) heat exchangers [14,15].

In recent reviews, it has been reported by different authors [16–19] that many configurations of flat plate PV/T collectors have been developed, either PVT/air or PVT/water. The main differences between the PV/T designs are whether a glass cover on a PV laminate is present [8,20] or not [21,22], the design of the sheet-and-tube collectors as round [3,5,20,23–25] or square/rectangular tube absorber type [26,27], and the type of the heat extracting fluid. PV/T systems with "one cover and no cover" effects were also investigated [2,28,29]. Whereas some of the researches focuses on component-based efficiency studies, some of the papers are focused on system-based applications regarding building heating/cooling [29–32] or water heating with or without a storage tank and auxiliary heating [3,33].

Authors who have studied these component-based models and verified the results by field or indoor experience stated that the achieved electrical efficiency is maximum for the uncovered collector, whereas the highest total electrical and thermal efficiency is obtained for a single-covered collector configuration due to the fact that thermal losses caused by convection decrease with a cover.

Several studies have followed up on the research and design of the water type PV/T collectors with one solar panel as the cover. It was reported in [4] that the hybrid PV/T system's total energy output is dependent on the solar energy input, ambient temperature, wind speed, operating temperature of the system parts, and heat extraction mode. Zondag et al. [5] pointed out that one of the main advantages of the PV/T system is the average PV temperature in a PV/T collector that might be lower than for a conventional PV-laminate, thereby increasing electrical performance.

PV/T hybrid collectors generate electrical energy beyond providing low temperature hot water. Thus, the total efficiency increases. Bergene and Lovvik [34] showed that the total theoretical efficiency of a PV/T collector that can be obtained is about 60–80%. Other test results stated that the thermal efficiency is about 50–70% [5]. The obtained results are, however, the instantaneous efficiencies, which are measured or calculated under constant and low input temperature fluid flow conditions.

Chow [7] stated an explicit dynamic model for the PV/T systems in contrast to most previous steady-state models and achieved a thermal efficiency of 60%. Ji et al. [30] also studied a dynamic thermal model

for the analysis of a façade-integrated photovoltaic/thermal collector system. Taking the dynamic parameters that affect the thermal and electrical efficiencies into account, they calculated the PV/T efficiency as 58.9% for the system using a thin film PV (EPV/T) and 60–80% for the system with a single silicon cell PV (BPV/T). Corbin and Zhai [35] stated that thermal and combined (thermal plus electrical) efficiencies reached 19% and 34.9% based on a computational ?uid dynamics model, respectively. In [35], the efficiency was calculated for a forced flow system where the fluid is circulated by a pump during daylight hours and a new correlation is developed that allows cell efficiency to be calculated directly.

If a storage tank is included in the PV/T system as in some studies [3,8,29,36], the input temperature in the closed system changes during the day. In such a system, as the inlet temperature is not constant during the day, the thermal efficiency should be stated according to daily test results.

In this work, the field of interest was the water type PV/T collector with a semitransparent solar module used as the cover. A storage tank was included in the system to provide a dynamic inlet water temperature as in an actual thermal collector. Forced circulation by a pump was experienced as well as natural circulation. The dynamic influences were taken into account in the developed model as the PV/T system was tested on the roof of the Ege University Solar Energy Institute building. Model equations were calculated via MATLAB and Simulink. The efficiency of the PV/T system was calculated according to outdoor daily test results, and the experimental results and model calculations are presented.

3. The PV/T hybrid system components

3.1. Solar modules

In the PV/T hybrid system, the solar module is integrated with the thermal collector, either by pasting the solar module onto the absorber plate of the collector or by placing them with an air gap. In these systems, the heat on the solar cells is the input of the thermal collector, which is transferred to the heat carrier fluid, but solar radiation is not incident on the absorber plate.

As some part of the incident solar radiation can be incident on the absorber plate, a thin-film amorphous semitransparent solar module (ASITHRU-30-SG) having a transparency of about 10% and a size of 60 $\times$ 100 cm^2 (Figure 1) was used. The electrical data of this module under standard test conditions (STC: 1000 W/m^2, AM 1.5, cell temperature 25 °C) after exposure to sunlight for a few months are given in Table 1.

Table 1. Electrical data and cell temperature coefficients of the solar module.

Nominal power	P_{MPP}	27 W_p
Voltage at the maximum power point	U_{MPP}	36 V
Current at the maximum power point	I_{MPP}	0.75 A
Short circuit current	I_{sc}	1.02 A
Open circuit voltage	U_{oc}	49 V
Number of series connected cells	N	30
Cell temperature coefficients		
Referred to nominal power	uP	–0.2%/K
Referred to open-circuit voltage	uU_{OC}	–0.33%/K
Referred to short-circuit current	uI_{SC}	+0.08%/K

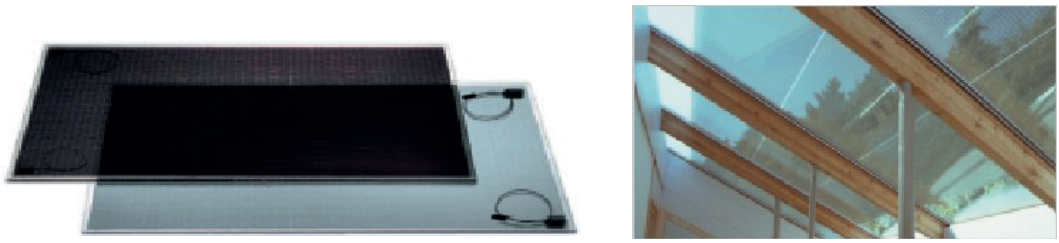

Figure 1. ASITHRU-30-SG semitransparent solar cell.

3.2. Thermal collector

The thermal collector used in the hybrid system is an active system which uses a 3-speed control pump to circulate a heat-transfer fluid between the collector and the storage tank. The performance of the system was also tested under natural flow conditions. The choice of the heat-transfer fluid was potable water as the system was tested in the mild climate of the city of İzmir. Polyurethane foam (50 mm) was used for the insulation of the collector and the tank, which prevented freezing and heat loss at night. On the absorber plate, there are 6 copper tubes of 12 mm in diameter having a space of 10 cm in between them, as shown in Figure 2. The thermal collector's absorber plate was coated with titanium dioxide (TINOX) of 0.2 mm thick in order to optimize the hybrid system's efficiency. This coating was chosen as the absorption level is higher than 95%, which increases the thermal output by 10% and reaches a higher plate temperature than the black absorber plate does.

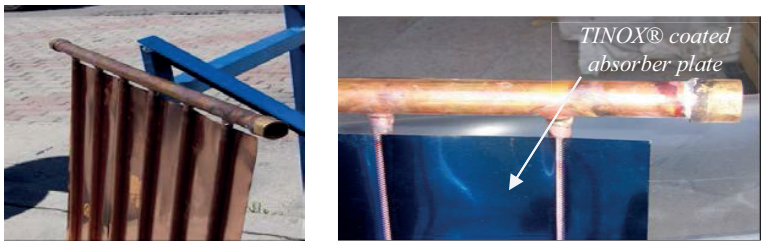

Figure 2. Construction details of the TINOX coated absorber plate.

3.3. Temperature, meteorological, and electrical measurements

The inlet and outlet water temperatures of the collector and the temperature of the storage tank were measured with 3 two-wire Metronik Pt-100 temperature sensors. The solar module's surface temperature was measured with two LM35 temperature sensors with 10 mV/°C sensitivity. The outputs of the temperature sensors were connected to a data logger via signal conditioning circuits and recorded with 10-min intervals. The microcontroller-based data logger was particularly designed for temperature sensor connections and analog inputs. The analog inputs were converted to digital with on-chip 16-bit analog-to-digital converters (SAR ADCs), which have a programmable throughput up to 1 Msps with a conversion time of about 100 *mu* s, and stored in a 128 Kbyte RAM memory. The data transfer to computer was performed via an EIA-232E communication port; the transfer was accomplished through HyperTerminal software, saved as text files, and then converted to comma-separated Microsoft Excel (*.csv) files. The current and voltage of the solar module under a load of 48 Ω was measured with a current sensor, CSA-1V, and a measuring circuitry, which was also stored in the data logger. The CSA-1V is a CMOS Hall sensor with an added ferromagnetic layer. The ferromagnetic layer is used as a magnetic flux concentrator providing a magnetic gain of about 10 to increase the output signal without increasing the inherent sensor electrical noise. The CSA-1V provides an analog output

voltage proportional to the magnetic field generated by the current flowing through a conductor near the IC. This sensor was used for on-board DC current measurements with very low insertion loss and fast response. Current-measuring circuitry, the data logger, and the sensor connections are shown in Figure 3. The measured meteorological data, including ambient temperature, solar radiation, and wind speed, were supplied by the Ege University Solar Energy Institute where the PV/T hybrid system was tested. These data was used for calculation of beam and diffuse components of hourly radiation on a tilted surface. The detailed features of the measuring and data logging units are given in Table 2.

Table 2. List of the measuring and data logging units.

Device	Specification	Value/feature
Pt-100 resistive temperature detector (RTD)	Sensor	Single sensor, 2-wire, thin-film
	Immersion length	50 mm for 2 RTDs, 100 mm for 1 RTD
	Nominal resistance	100 Ω @ 0 °C (IEC751 standard, Class B)
	TCR (IEC751)	$\alpha_0 = 3.85 \times 10^{-3\circ}\mathrm{C}^{-1}$ from 0 to 100 °C
	Temperature range	–50 to +500 °C
LM35 temperature sensor	Calibration	in °C
	Output	Linear 10.0 mV/°C scale factor
	Accuracy	0.5 °C (at +25 °C)
	Rated for full range	–55 to +150 °C
	Nonlinearity	± $^1/_4$ °C typical
CSA-1V current sensor - low current range properties	Electrical noise	Low
	DC offset voltage	± 15 mV max
	Working current range	Up to 2 A
	Signal output	140 mV for 1 A
	Resolution	Approx. 5 mA
	Linearity	<1%
Microcontroller-based data logger	3 Pt-100 temperature sensor inputs	
	Two 0 to 10 mV, two 0 to 2.5 V, and one 0 to 1 V analog inputs	
	128 Kbyte data storage capacity	
	16 bit resolution on-chip SAR ADC, conversion time: 100 mu s	
	2 × 16 character LCD display	
	1 to 256 min user-adjustable range for data logging	
	Instantaneous value display on LCD	
Meteorology station	Solar radiation sensor	0 to 1800 W/m^2; accuracy ± 5% FS
	Anemometer with direction	1 to 322 km/h
	Precision thermistor	–40 to +65 °C; accuracy ± 0.5 °C

4. Design and experimental study of the PV/T hybrid system

In the experimental study, the solar module and the absorber plate were placed with a spacing of 2 cm and the hybrid PV/T system was observed under forced and natural circulation conditions. In this system, as shown in

Figure 4, the solar module, which is 10% transparent to sunlight, was used as the cover of the thermal collector. Most of the incoming solar radiation was absorbed and converted into electrical energy by the solar module and a small portion was incident on the absorber plate. Electrical efficiency and the effect of temperature on the efficiency were observed. With the aid of the PV/T system's mathematical modeling in [5,34,37], the thermal part was modeled. Experimental results and calculated results from the model were then compared.

Figure 3. Current measuring circuit, data logger, and temperature sensor connections.

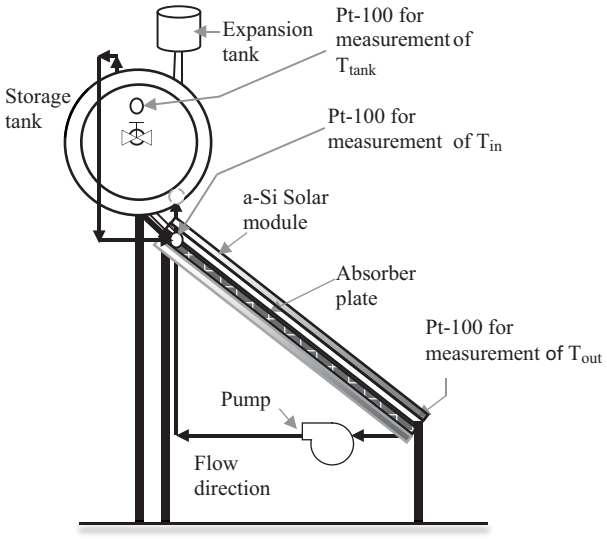

Figure 4. Schematic drawing of the PV/T system.

Electrical efficiency under STC was calculated as:

$$\eta_0 = \frac{V_{MPP} \cdot I_{MPP}}{G \cdot A_{PV}} \tag{1}$$

Electrical efficiency as a function of temperature is defined as in Eq. (2) [37], and the temperature coefficient –0.45% $^{\circ}C^{-1}$ for monocrystalline silicon was replaced with –0.2% $^{\circ}C^{-1}$ for amorphous silicon. Using this equation and the surface temperatures of the solar module, the temperature dependence of the solar module was analyzed.

$$\eta_e = \eta_0(1 - 0.002[T_{cell} - 25^{\circ}C]) \tag{2}$$

5. Solar radiation on a tilted surface

For evaluation of the electrical and thermal efficiencies, the measured solar radiation and wind speed data were used. As the meteorology station measures the solar radiation on the horizontal plane, the radiation onto the tilted surface was calculated for the PV/T system facing south with a slope equal to İzmir's latitude ($\beta = \Phi = 38.46^{\circ}$). The hourly total radiation received on a tilted surface $I_{T,\beta}$ is the sum of the hourly beam irradiation $I_{b,\beta}$, the hourly reflected irradiation $I_{r,\beta}$, and the hourly sky diffuse radiation on the tilted surface $I_{d,\beta}$, which is composed of 3 parts: isotropic, circumsolar diffuse, and horizon brightening.

For the PV/T system facing south ($\gamma = 0^{\circ}$) calculated hour angles (ω) and declination angles (δ) were used to compute the hourly beam radiation component from the measured solar radiation using the model of Erbs et al. [37,38].

The diffuse radiation component on the tilted surface was calculated using the anisotropic estimation model of Perez [37,39] as it is the most used model with an accuracy of better than 10%. The equations in the Perez model were utilized to calculate the 3 components of the diffused radiation on a tilted surface. By adding the beam and the ground-reflected radiation, the total radiation was calculated as [39]:

$$I_{T,\beta} = I_b R_b + I_d(1-F_1)\left(\frac{1+\cos\beta}{2}\right) + I_d F_1 \frac{a}{b} + I_d F_2 \sin\beta + I\rho_g\left(\frac{1-\cos\beta}{2}\right) \tag{3}$$

The brightness coefficients F_1 and F_2 are functions of the zenith angle θ_z, clearness ε as described in [39], and brightness Δ.

A simulation program, Simulink, was used to calculate the hourly radiation on a tilted surface for any day changing the number of the day, n, using the measured hourly solar radiation data and the results presented in [40].

6. Energy balance equations for the PV/T system

In this model, the PV/T system studied was a flat-plate collector with a semitransparent solar module on top serving as the cover of the collector. The absorber plate of the flat-plate collector was designed so that the cylindrical copper tubes were in good contact with the plate. For the absorber plate, a highly selective titanium dioxide coating was used to ensure the greatest possible degree of absorption within the solar radiation range and the lowest possible degree of emissivity in the heat radiation range. Therefore, with the TINOX selective coating, heat losses due to heat radiation from the absorber plate were prevented in the infrared range.

Rather than considering the photovoltaic and thermal parts separately, it was more convenient to model the system as one unit affected by each. Energy balance equations were written for the flat-plate collector where, instead of a glass cover, a thin film a-Si solar module in between 2 glasses was used (Figure 5).

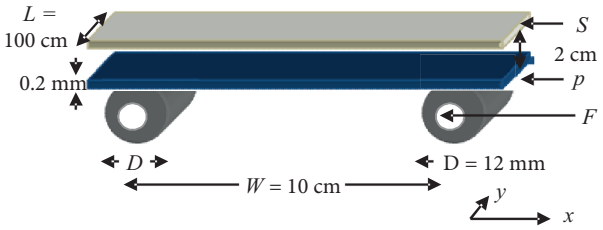

Figure 5. Geometric configuration and dimensions of the hybrid system model.

In the modeling, the effect of the change in hourly solar radiation and the effect of wind speed on the performance of the PV/T system were considered for more accurate results, so the measured solar radiation, temperature, and wind speed data were used.

In the geometrical configuration of the system shown in Figure 5, the Hottel–Whillier model was referenced and some modifications were made due to the fact that the glass cover in that model was replaced by a semitransparent thin-film a-Si solar module of 10 mm in thickness and the energy losses due to radiation and convection from the 3 mm top glass of the module were taken into consideration [41].

Heat losses from the solar module due to convection may be a combination of free and forced convection effects. When the front of the module is exposed to wind, forced convection will be the main cause of cooling [41]. As a result, the overall convection heat transfer is the sum of the forced convection from the front surface

and the free convection from the rear surface. In this study, as the PV module is used for the glass cover placed approximately 2.5 cm apart from the absorber plate, there is no cooling effect at the rear surface caused by free convection. Heat losses from the top glass of the solar module due to convection caused by wind should be taken into consideration as the PV module was used for the glass cover of the collector. McAdams' (1954) empirical heat transfer coefficient, $h_{wind} = 5.7 + 3.8 v_{wind}$, was used for calculating the convective heat transfer coefficient. For evaluation of the top loss coefficient U_t, the empirical formula of Klein in [37] was used, whereas the calculations were done by a simulation software program [40].

There is a conductive heat transfer from the absorber plate to the case of the collector via insulation material, so the bottom heat loss coefficient U_b was calculated as:

$$U_b = \frac{k}{L_{ins}} \tag{4}$$

Edge loss coefficient U_e was also calculated as the edge loss coefficient-area product $(UA)_{edge}$ to the collector area A_c:

$$U_e = \frac{(UA)_{edge}}{A_c} \tag{5}$$

The collector overall loss coefficient, U_L, is the sum of all these losses.

Tube-and-fin model [37] was used to find the heat conducted from the fin to the tube via the absorber plate. Using the useful gain for the tube and fin per unit length in the flow direction $q_u^{'}$, energy transferred from the absorber plate to the fluid through the tubes was then calculated to find out how efficiently the collector, and thus the PV/T system would work.

The fin, shown in Figure 6, is of length $(W - D)/2$. An energy balance on the elemental region of width Δx and unit length in the flow direction is found to be:

$$q'_{fin} = (W - D)F[S - U_L(T_b - T_a)] \tag{6}$$

where S is the absorbed solar radiation by the unit area of the absorber plate $(\mathrm{J/m^2})$, T_b is the bond temperature, and F is the fin efficiency:

$$F = \frac{\tanh[m(W - D)/2]}{m(W - D)/2} \tag{7}$$

which is defined as the measure of how efficiently the heat is transferred from the fin to the tube via the absorber plate, where $m = \sqrt{U_L/k\delta}$, k is the thermal conductivity of TINOX coating, and δ is the absorber thickness.

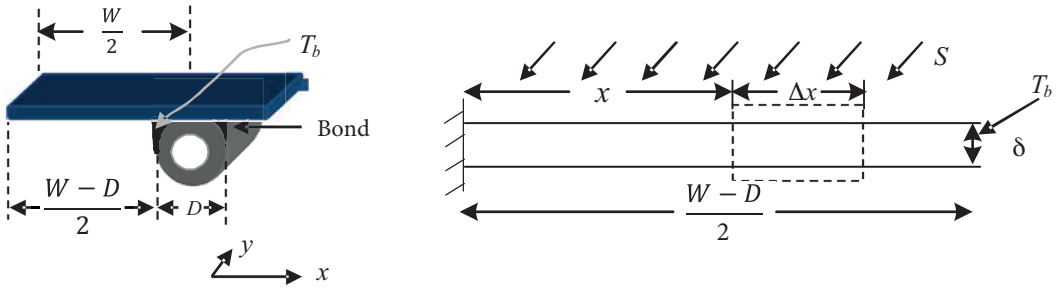

Figure 6. Energy balance on the fin element.

The useful gain that can be obtained from the absorber plate for the tube is

$$q'_{tube} = D \cdot [S - U_L(T_b - T_a)] \tag{8}$$

and the useful gain for the tube and fin per unit length in the flow direction is the sum of Eqs. (6) and (8):

$$q'_u = [(W - D)F + D][S - U_L(T_b - T_a)] \tag{9}$$

This useful gain should be transferred to the fluid. The useful gain can be expressed in terms of the resistance to heat flow to the fluid that results from the bond and the tube-to-fluid resistance.

$$q'_u = \frac{(T_b - T_{fi})}{\frac{1}{h_{fi}\pi D_i} + \frac{1}{C_b}} \tag{10}$$

where D_i is the inner diameter of the tube, h_{fi} is the heat transfer coefficient between the fluid and the tube wall, T_{fi} is the temperature of the fluid entering the fin, and C_b is the bond conductance. As the tubes were bonded to the absorber plate by ultrasonic seam welding, which provides low thermal load, the bond resistance $(1/C_b)$ was neglected.

T_b should be preferably eliminated from the equations in order to obtain an expression for the useful gain in terms of measurable physical parameters. Solving Eq. (14) for T_b, substituting into Eq. (9), and solving for the useful gain, we have:

$$q'_u = W \cdot F'[S - U_L(T_{fi} - T_a)] \tag{11}$$

where $F\prime$ is the collector efficiency factor.

The quantity that relates the actual useful energy gain of a collector to the useful gain is called the collector heat removal factor, F_R, and in equation form is:

$$F_R = \frac{\dot{m}C_p}{A_c U_L}\left[1 - \exp\left(-\frac{A_c U_L F'}{\dot{m}C_p}\right)\right] \tag{12}$$

where $\dot{m}$ is the total collector flow rate in kg/s.

The collector heat removal factor, F_R, is used to calculate the useful energy gain Q_u as:

$$Q_u = A_c F_R[S - U_L(T_{in} - T_a)] \tag{13}$$

Instead of inlet fluid temperature T_{fi} notation, T_{in} notation is used because of the fact that inlet water temperature is being measured in this system. However, losses based on the inlet fluid temperature are very small due to the fact that most of the losses occur along the collector from the plate where the temperature increases in the flow direction.

The measured values are used in determining the thermal system's actual efficiency as:

$$\eta_{th} = \frac{\dot{m}C_p(T_{out} - T_{in})}{A_c \cdot G} \tag{14}$$

where collector inlet and outlet temperatures T_{in} and T_{out} were measured and the solar radiation on the tilted plane was calculated using the measured solar data. Collector area A_c is equal to the solar module area. When

the system works in natural circulation, the flow rate, $\dot{m}$, changes with the difference between T_{in} and T_{out}. This average flow rate in the closed loop in m/s is calculated using temperature difference by [42]:

$$v_m = (g\beta' Q_u H / 8\mu L \pi C_p)^{1/2} \tag{15}$$

The useful heat Q_u transferred from the tubes to the fluid is calculated as:

$$Q_u = \dot{m} C_p (T_{out} - T_{in}) \tag{16}$$

and placed into Eq. (15). The unknown mass flow rate in Eq. (16) was solved using:

$$\dot{m} = \rho v_m A_{tube} \tag{17}$$

An iterative method was used to solve for v_m, and $\dot{m}$ is calculated consequently.

The mathematical model of the collector part of the PV/T system was designed in MATLAB and the flowchart is given in Figure 7.

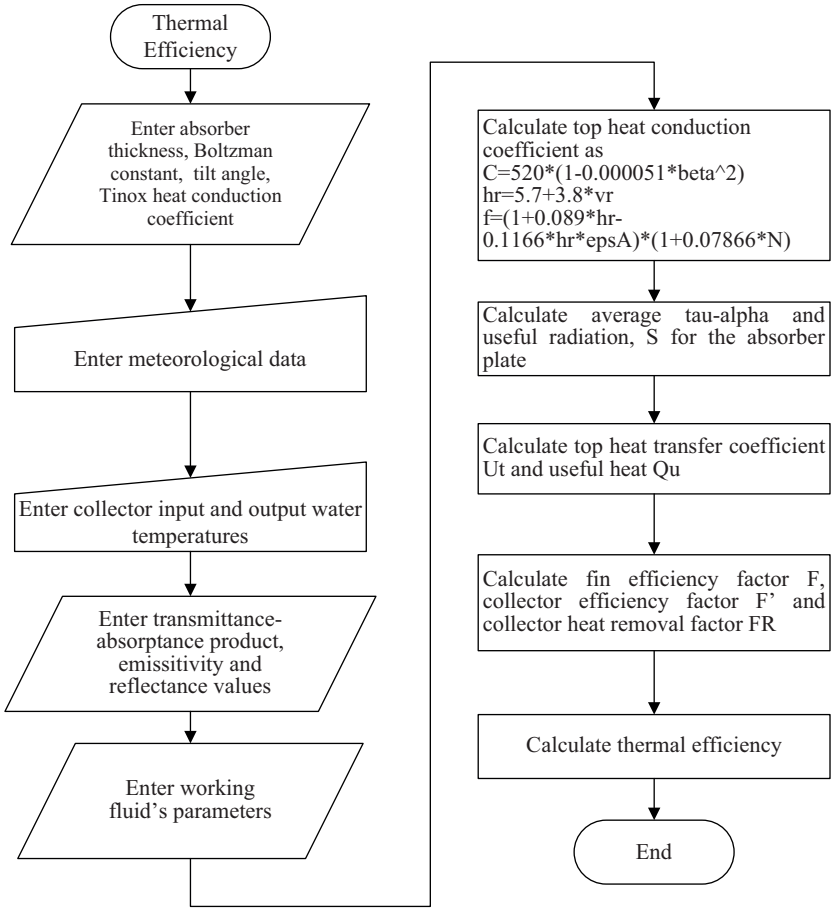

Figure 7. Flowchart for thermal efficiency model.

7. a-Si solar module model

The solar module's electrical characteristic is affected by the collector fluid temperature. The 3 mm top glass of the module causes optical losses due to reflections. However, the degradation in the electrical efficiency due to the optical losses is smaller than the increase in efficiency due to the solar cell crystal temperature decrease.

Integration of the solar module and the thermal collector changes the characteristics of both, so the electrical part should also be modeled in order to investigate the system completely.

In a solar cell, the recombination in the depletion region represents a considerable loss, which cannot be sufficiently modeled using a single diode model [43]. Therefore, the a-Si solar module is modeled using the two-diode PV model in [44], and the equations in [45] are adapted to this model.

The two-diode PV model in Figure 8 was used due to the fact that the a-Si PV cell has a large series resistance, R_s, and the recombination current is substantially high, both of which were taken into consideration in the referenced model. Recombination current also directly affects the fill factor (FF) of the PV cell and thus has a significant effect on the open-circuit voltage, V_{oc} [46].

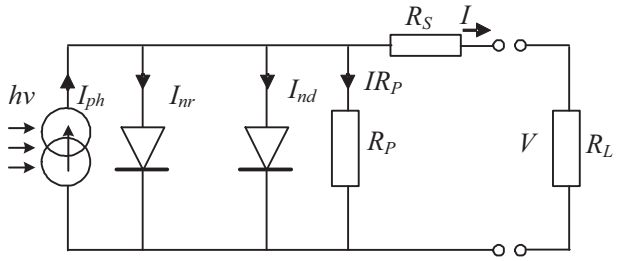

Figure 8. The a-Si PV two-diode model.

In this model, the PV cell's dark current, I_0, can be stated in terms of diffusion current I_{0d} and recombination current I_{0r} as:

$$I_0 = I_{0d}\left[\exp(V/V_{td0}) - 1\right] + I_{0r}\left[\exp(V/V_{tr0}) - 1\right] \tag{18}$$

where $V_{td0} = n_d kT_{c0}/qandV_{tr0} = n_r kT_{c0}/q$. n_d and n_r are diode ideality factors, k is the Boltzmann constant, and q is the electron charge.

The first diode represents the dark recombination current while the second represents the diffusion current. In the equivalent circuit model, resistor R_P represents high-conductivity paths through the solar cell caused by crystal damage in the junction. The resistor R_S represents the series resistance in the top surface of the semiconductor and at the metal contact-to-semiconductor interface [44].

Eq. (18) may be rewritten taking into consideration these resistances as:

$$I_0 = I_{0d}\left[\exp((V + IR_S)/V_{td0}) - 1\right] + I_{0r}\left[\exp((V + IR_S)/V_{tr0}) - 1\right] + (V + IR_S)/R_P \tag{19}$$

R_P, in practice, has a very large value, though the current it draws is neglected in order to minimize the calculation period in computer-based modeling. Therefore, by neglecting the last term in Eq. (19), the net current that can be drawn from the circuit is the difference between photocurrent I_{ph} and dark current as:

$$I_{PV} = I_{ph} - I_0 = I_{ph} - \{I_{0d}\left[\exp(V + IR_S/V_{td0}) - 1\right] + I_{0r}\left[\exp(V + IR_S/V_{tr0}) - 1\right]\} \tag{20}$$

The photocurrent depends on solar irradiation and temperature as indicated in Eq. (21):

$$I_{ph} = (G/G_0)\left[(I_{sc0} + uI_{sc}(T_c - T_{cref})\right] \tag{21}$$

A solar cell mathematical model was implemented in MATLAB and cell parameters were obtained from reference module parameters, and cell parameters were calculated and investigated as solar irradiation- and temperature-dependent parameters under nominal working conditions. The dark current of the solar cell was calculated to

find the PV current as in Eq. (20). Solar cell efficiency (η_0), FF, and R_S were also calculated. The flowchart for this model is given in Figure 9. By increasing the voltage values from 0 to open circuit voltage, I-V curves were obtained for one cell of the module for various radiations and temperatures as given in Figure 10. In these calculations equations from [45] were used. The I-V curve in Figure 10 is obtained for one cell; therefore, the module voltage is 30 times the cell voltage. The obtained curve approximates the ideal curve as series resistance was neglected for low currents.

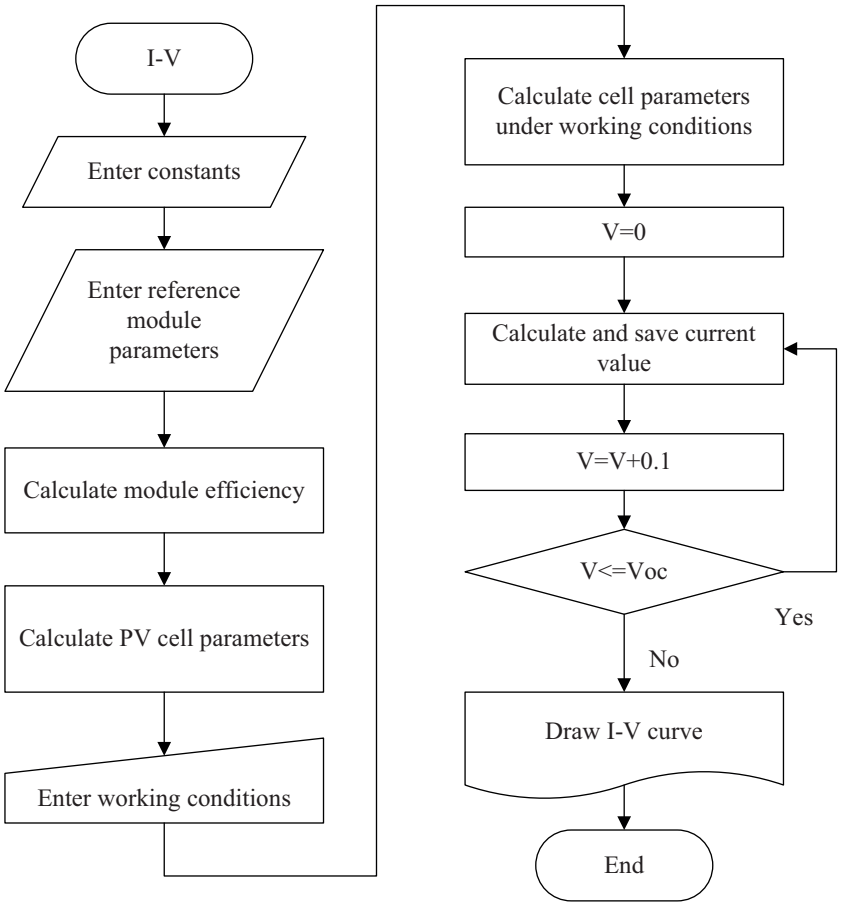

Figure 9. Flowchart of PV cell model.

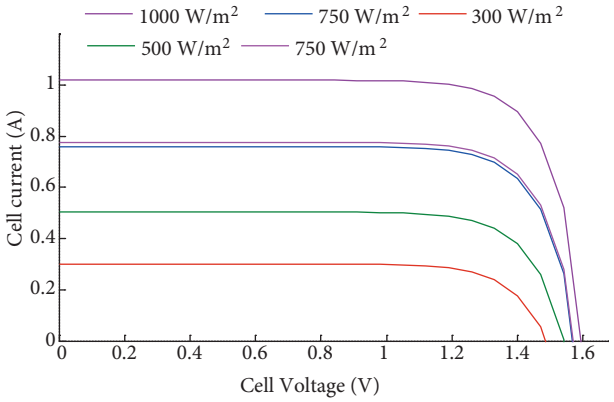

Figure 10. The I-V curve of the cell obtained for various solar radiations.

8. Results and discussion

The PV/T hybrid system was installed, the measuring system was connected, and an outdoor test was implemented. In this system, the PV module, which is 10% transparent to sunlight, was used as the cover of the thermal collector. Most of the incoming solar radiation was absorbed and converted into electrical energy by the solar module and a small portion was incident on the absorber plate. The measured collector input (T_{in}) and output (T_{out}) water temperatures, the storage tank temperature (T_{tank}), the surface temperatures of the solar module (T_{s1},T_{s2}), and the ambient temperature (T_a) variations of the PV/T hybrid system on August 12 are shown in Figure 11.

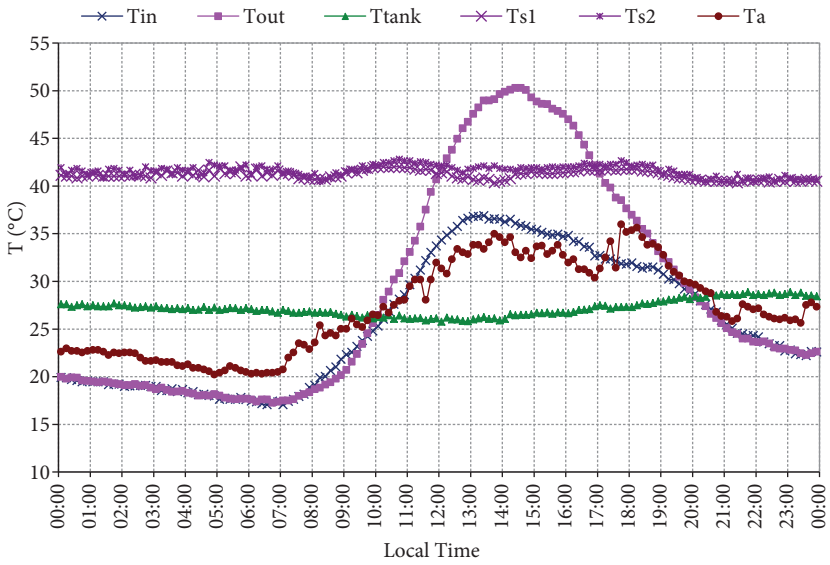

Figure 11. Measured temperatures of the PV/T hybrid system for August 12.

Measured electrical parameters of the PV/T hybrid system and the meteorological data are plotted versus time for the same day in Figures 12 and 13, respectively.

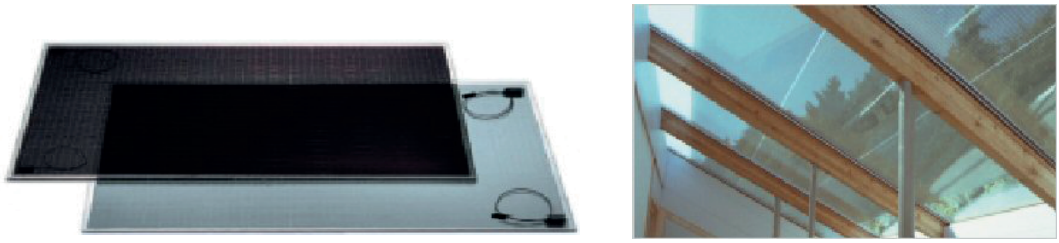

Figure 12. Measured module current, voltage, and ambient temperature.

It can be inferred from the measurements that the PV/T system's collector outlet water temperature slightly exceeds 50 °C, and heat was transferred to the water in the collector part. The difference between inlet and outlet water temperatures was about 14 °C for the natural flow through the system. Water temperature in the tank exceeded 28 °C and remained almost constant during the day although the warm water was used by the consumer. This 1-day data can be verified for the measured water temperatures for a period between August 20 and August 24 as shown in Figure 14.

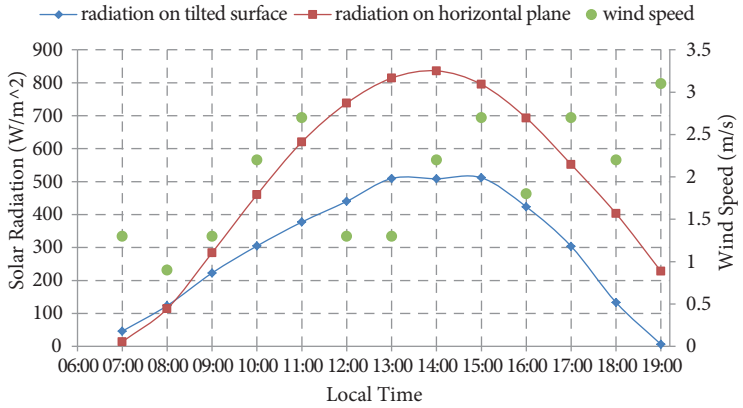

Figure 13. Wind speed and solar radiation variations on August 12.

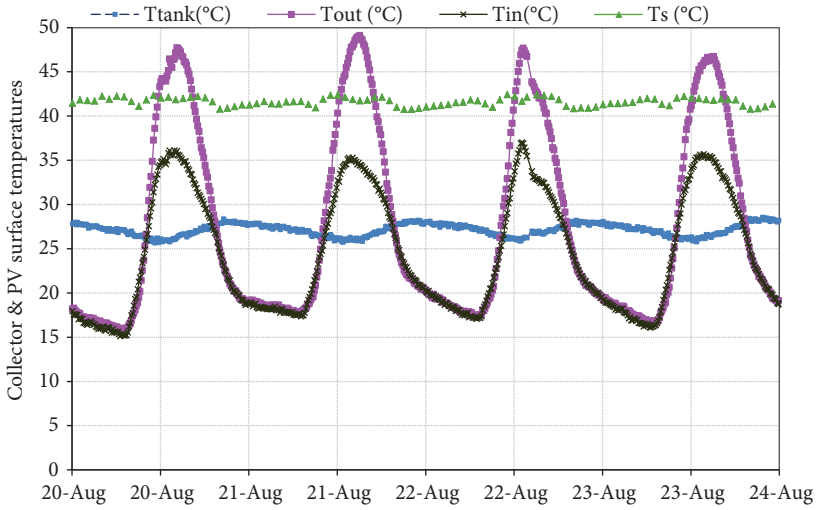

Figure 14. Water temperatures for August 20–24 for the PV/T system.

The solar module's surface temperatures, measured from two distinct places, did not exceed 40 °C, even during the sunshine duration, and remained almost constant during the day. As is shown in the meteorological data graphic (Figure 13), wind speed reached at most 3.1 m/s and remained under 1.5 m/s during the day, so forced convection had very little effect on the heat loss of the solar module surface.

In the experimental setup, a current through a 48 Ω load increases the PV module cell temperature whereas water flow through the collector decreases this temperature. For comparison with the no-load condition, the load was disconnected, the solar module voltage rose to approximately $U_{oc} = 49$ V @ STC, and the current dropped to zero. The test results for load/no-load conditions are given in Figure 15.

The PV/T system was also operated under forced circulation conditions and the tank temperature reached higher values, and heat transfer to the tank was accomplished.

The semitransparent solar module with 10% transparency was demounted from the system, and the system was separated into 2 parts as a solar module and a thermal collector with a glass cover as shown in Figure 16. Water temperatures were examined for the data from August 26 to 31, where the hot water flowing through the collector tubes reached 80 °C for the thermal collector working with a glass cover, as shown in Figure 17. The water temperature for the PV/T system could not reach the high values that the thermal collector did, due to the shading of the absorber plate by the solar module.

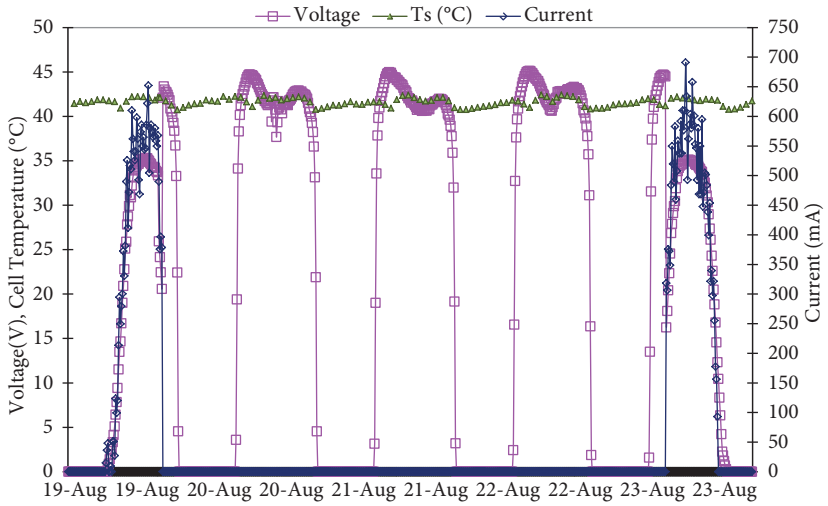

Figure 15. Voltage and current variations for load/no-load conditions for the PV module.

Figure 16. Thermal collector and solar module under test.

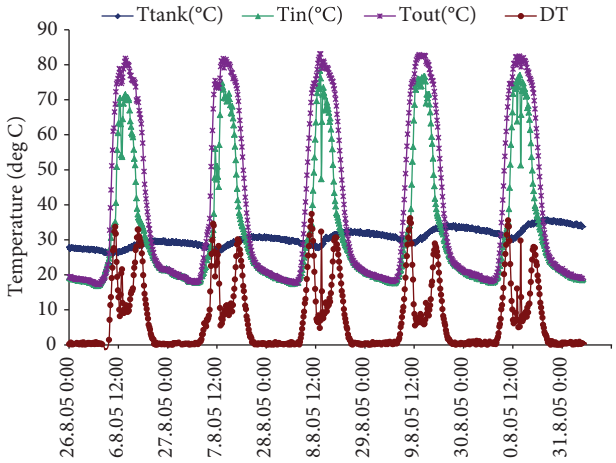

Figure 17. Water temperatures from August 26 to 31 for thermal part.

The measured voltage and current values for August 27 are plotted in Figure 18. The voltage and current values verify that the solar module worked at the MPP for this day, improving the electrical efficiency to the maximum.

The collector temperatures under natural and forced circulation conditions were tested. It was observed that collector temperatures reached higher values of about 10 °C for forced circulation with a pump. This mode of operation also enhanced the heat transfer to the storage tank where the water temperature in the tank almost reached the temperature of the water through the collector tubes. When the system works in natural circulation mode, the flow rate changes with the temperature difference $(T_{out} - T_{in})$. Thermal efficiency versus reduced temperature, $(T_{in} - T_a)/G$, is plotted as shown in Figure 19.

The effect of cell temperature on electrical efficiency was observed and the results are given in Figure 20. It was concluded that as the temperature coefficient of the a-Si PV module has a lower value than the monocrystalline Si PV module; cooling the PV laminate did not affect the electrical efficiency as expected.

However, the choice of a semitransparent module increased the solar radiation reaching the absorber plate and thus increased the thermal efficiency.

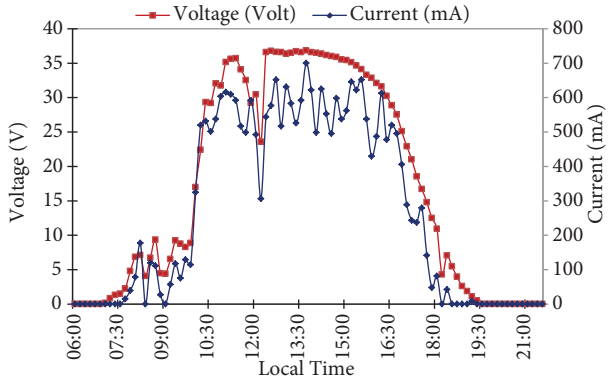

Figure 18. Module current and voltage variations for a-Si solar module for August 27.

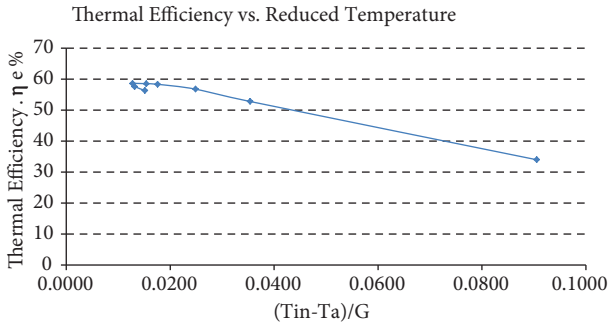

Figure 19. Thermal efficiency vs. reduced temperature.

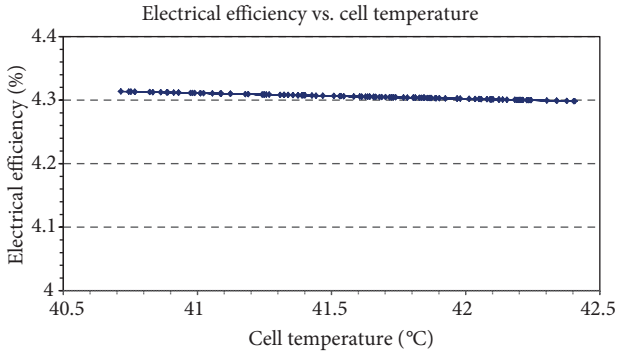

Figure 20. Electrical efficiency vs. cell temperature.

The obtained results from this special design were compared with the previous studies for both electrical and thermal efficiencies. The thermal efficiency for the thermal part was measured to be 52% with an electrical efficiency of 4.2%, giving an overall efficiency of 56.2%. Some of the PV/T systems were designed specially with considerably higher efficiencies. In this study, the PV/T system was constructed with commercially available products, and hence the thermal and electrical efficiencies are compared with similar designs. When compared to the obtained efficiencies $\eta_e = 0.06$ and $\eta_{th} = 0.60 - 12.02\ (\Delta T/G)$ in [4], the thermal efficiency is found to be ˜10% higher due to the improvements in the collector design. The a-Si module's efficiency in the study of the authors was 6%, whereas the semitransparent a-Si module's efficiency was 4.2% in the designed PV/T system. The other obtained PV/T overall efficiencies and electrical efficiencies in the literature are 34.9% and 5.3% [35], 38% and 9% [3], 54% and 9.7% [5], and 58.9% and 4.3%, respectively [30]. A PV module with higher efficiency could be used for providing higher overall (thermal + electrical) efficiency, but at the time the system was designed a semitransparent module with higher efficiency could not be obtained from the market.

9. Conclusion

A PV/T system with a semitransparent a-Si solar module used as the cover of the thermal collector was designed and constructed. The solar module's electrical efficiency was determined by measuring cell temperatures with

temperature sensors and the current and the voltage by a current sensor via a circuit. Experimentally, the electrical efficiency was measured to be 4.35%, which is close to the stated efficiency of the manufacturer, and was calculated to be 4.41% from the model.

The PV/T hybrid system efficiency was compared to the solar module and the thermal collector efficiencies when operated separately. The thermal collector, operated in natural circulation mode, has a thermal efficiency of 41%, whereas the efficiency was 58.7% during forced circulation with a pump. The PV/T hybrid system's instantaneous efficiency under natural flow conditions was found to be 71%. The PV/T system's daily thermal efficiency for forced circulation was calculated to be 59.5% by the model, whereas the measured efficiency for the same day was 52%. Due to the selection of a semitransparent PV module and the TINOX coating of the absorber plate with high absorption level, the overall efficiency of the PV/T hybrid system was improved, and the obtained efficiency is close to or higher than the ones given in the literature as discussed in Section 5.

References

[1] Garg H, Agarwal R. Some aspects of a PV/T collector/forced circulation flat plate solar water heater with solar cells. Energ Convers Manage 1995; 36: 87-99.

[2] Fujisawa T, Tani T. Annual exergy evaluation on photovoltaic-thermal hybrid collector. Sol Energ Mat Sol C 1997; 47: 135-148.

[3] Huang B, Lin T, Hung W, Sun F. Performance evaluation of solar photovoltaic/thermal systems. Sol Energy 2001; 70: 443-448.

[4] Tripanagnostopoulos Y, Nousia T, Souliotis M, Yianoulis P. Hybrid photovoltaic/thermal solar systems. Sol Energy 2002; 72: 217-234.

[5] Zondag HA, de Vries DW, van Helden WGJ, van Zolingen RJC, van Steenhoven AA. The thermal and electrical yield of a PV-thermal collector. Sol Energy 2002; 72: 113-128.

[6] Zondag HA, de Vries DW, van Helden WGJ, van Zolingen RJC, van Steenhoven AA. The yield of different combined PV-thermal collector designs. Sol Energy 2003; 74: 253-269.

[7] Chow T. Performance analysis of photovoltaic-thermal collector by explicit dynamic model. Sol Energy 2003; 75: 143-152.

[8] Chow TT, He W, Ji J. Hybrid photovoltaic-thermosyphon water heating system for residential application. Sol Energy 2006; 80: 298-306.

[9] Sopian K, Yigit K, Liu H, Kakac S, Veziroglu T. Performance analysis of photovoltaic thermal air heaters. Energ Convers Manage 1996; 37: 1657-1670.

[10] Garg HP, Adhikari RS. System performance studies on a photovoltaic/thermal (PV/T) air heating collector. Renew Energ 1999; 16: 725-730.

[11] Hegazy AA. Comparative study of the performances of four photovoltaic/thermal solar air collectors. Energ Convers Manage 2000; 41: 861-881.

[12] Aste N, Chiesa G, Verri F. Design, development and performance monitoring of a photovoltaic-thermal (PVT) air collector. Renew Energ 2008; 33: 914-927.

[13] Tonui J, Tripanagnostopoulos Y. Performance improvement of PV/T solar collectors with natural air flow operation. Sol Energy 2008; 82: 1-12.

[14] Assoa Y, Menezo C, Fraisse G, Yezou R, Brau J. Study of a new concept of photovoltaic–thermal hybrid collector. Sol Energy 2007; 81: 1132-1143.

[15] Tripanagnostopoulos Y. Aspects and improvements of hybrid photovoltaic/thermal solar energy systems. Sol Energy 2007; 81: 1117-1131.

[16] Charalambous P, Maidment G, Kalogirou S, Yiakoumetti K. Photovoltaic thermal (PV/T) collectors: a review. Appl Therm Eng 2007; 27: 275-286.

[17] Zondag HA. Flat-plate PV-thermal collectors and systems: a review. Renew Sust Energ Rev 2008; 12: 891-959.

[18] Chow T. A review on photovoltaic/thermal hybrid solar technology. Appl Energ 2010; 87: 365-379.

[19] Ibrahim A, Othman MY, Ruslan MH, Mat S, Sopian K. Recent advances in flat plate photovoltaic/thermal (PV/T) solar collectors. Renew Sust Energ Rev 2011; 15: 352-365.

[20] De Vries DW, Van Helden WGJ, Van Steenhoven RJ, Van Zoligen RJ, Smuders PT. Design of a photovoltaic/thermal hybrid panel: design considerations and preliminary model. In: ISES EuroSun '96 Conference; 16–19 September 1996; Freiburg, Germany. pp. 623-628.

[21] Muresan C, Ménézo C, Bennacer R, Vaillon R. Numerical simulation of a vertical solar collector integrated in a building frame: radiation and turbulent natural convection coupling. Heat Transfer Eng 2006; 27: 29-42.

[22] Krauter S, Araújo RG, Schroer S, Hanitsch R, Salhi MJ, Triebel C, Lemoine R. Combined photovoltaic and solar thermal systems for facade integration and building insulation. Sol Energy 1999; 67: 239-248.

[23] Bakker M, Zondag HA, Elswijk MJ, Strootman KJ, Jong MJM. Performance and costs of a roof-sized PV/thermal array combined with a ground coupled heat pump. Sol Energy 2005; 78: 331-339.

[24] Santbergen R, Rindt C, Zondag H, Van Zolingen R. Detailed analysis of the energy yield of systems with covered sheet-and-tube PVT collectors. Sol Energy 2010; 84: 867-878.

[25] Charalambous P, Kalogirou S, Maidment G, Yiakoumetti K. Optimization of the photovoltaic thermal (PV/T) collector absorber. Sol Energy 2011; 85: 871-880.

[26] Sandnes B, Rekstad J. A photovoltaic/thermal (PV/T) collector with a polymer absorber plate. Experimental study and analytical model. Sol Energy 2002; 72: 63-73.

[27] Cristofari C, Notton G, Canaletti JL. Thermal behavior of a copolymer PV/Th solar system in low flow rate conditions. Sol Energy 2009; 83: 1123-1138.

[28] Morita Y, Fujisawa T, Tani T. Moment performance of photovoltaic/thermal hybrid panel (numerical analysis and exergetic evaluation). Electr Eng Jpn 2000; 133: 43-51.

[29] Fraisse G, Ménézo C, Johannes K. Energy performance of water hybrid PV/T collectors applied to combisystems of direct solar floor type. Sol Energy 2007; 81: 1426-1438.

[30] Ji J, Chow TT, He W. Dynamic performance of hybrid photovoltaic/thermal collector wall in Hong Kong. Build Environ 2003; 38: 1327-1334.

[31] Vokas G, Christandonis N, Skittides F. Hybrid photovoltaic–thermal systems for domestic heating and cooling—a theoretical approach. Sol Energy 2006; 80: 607-615.

[32] Eicker U, Dalibard A. Photovoltaic–thermal collectors for night radiative cooling of buildings. Sol Energy 2011; 85: 1322-1335.

[33] Dupeyrat P, Ménézo C, Rommel M, Henning HM. Efficient single glazed flat plate photovoltaic–thermal hybrid collector for domestic hot water system. Sol Energy 2011; 85: 1457-1468.

[34] Bergene T, Løvvik OM. Model calculations on a flat-plate solar heat collector with integrated solar cells. Sol Energy 1995; 55: 453-462.

[35] Corbin CD, Zhai ZJ. Experimental and numerical investigation on thermal and electrical performance of a building integrated photovoltaic–thermal collector system. Energ Buildings 2010; 42: 76-82.

[36] Dubey S, Tiwari G. Thermal modeling of a combined system of photovoltaic thermal (PV/T) solar water heater. Sol Energy 2008; 82: 602-612.

[37] Duffie JA, Beckman WA. Solar Engineering of Thermal Processes. 2nd ed. New York, NY, USA: Wiley, 1991.

[38] Notton G, Cristofari C, Poggi P, Muselli M. Calculation of solar irradiance profiles from hourly data to simulate energy systems behaviour. Renew Energ 2002; 27: 123-142.

[39] Notton G, Cristofari C, Poggi P. Performance evaluation of various hourly slope irradiation models using Mediterranean experimental data of Ajaccio. Energ Convers Manage 2006; 47: 147-173.

[40] Engin D, Engin M. Simulation modelling of a photovoltaic and thermal collector (PV/T) hybrid system. In: 6th International Ege Energy Symposium and Exhibition; 28–30 June 2012; İzmir, Turkey. pp. 471-482.

[41] Jones A, Underwood C. A thermal model for photovoltaic systems. Sol Energy 2001; 70: 349-359.

[42] Başaran T. Kapalıtermosifon döngüsünde akış ve ısıtransferinin teorik ve deneysel incelenmesi. PhD, Dokuz Eylül University, İzmir, Turkey, 2002 (in Turkish).

[43] Ishaque K, Salam Z, Taheri H. Simple, fast and accurate two-diode model for photovoltaic modules. Sol Energ Mat Sol C 2011; 95: 586-594.

[44] Stutenbaeumer U, Mesfin B. Equivalent model of monocrystalline, polycrystalline and amorphous silicon solar cells. Renew Energ 1999; 18: 501-512.

[45] Hansen AD, Sørensen P, Hansen LH, Bindner H. Models for a stand-alone PV system. In: Madsen PH, Lundsager P, editors. Proceedings of UNDTCD/Danida/Risø International Workshop on Wind Energy. Roskilde, Denmark: Danka Services International A/S, 2001.

[46] Zambrano RJ, Rubinelli FA, Arnoldbik WM, Rath JK, Schropp RE. Computer-aided band gap engineering and experimental verification of amorphous silicon–germanium solar cells. Sol Energ Mat Sol C 2004; 81: 73-86.